Swansea University
Prifysgol Abertawe

Cronfa
Setting Research Free

Cronfa - Swansea University Open Access Repository

This is an author produced version of a paper published in :
ACS Applied Materials & Interfaces

Cronfa URL for this paper:
http://cronfa.swan.ac.uk/Record/cronfa29930

Paper:
Kryvchenkova, O., Abdullah, I., Macdonald, J., Elliott, M., Anthopoulos, T., Lin, Y., Igi, P., Kalna, K. & Cobley, R. (2016). Nondestructive Method for Mapping Metal Contact Diffusion in In2O3Thin-Film Transistors. *ACS Applied Materials & Interfaces, 8*(38), 25631-25636.
http://dx.doi.org/10.1021/acsami.6b10332

This article is brought to you by Swansea University. Any person downloading material is agreeing to abide by the terms of the repository licence. Authors are personally responsible for adhering to publisher restrictions or conditions. When uploading content they are required to comply with their publisher agreement and the SHERPA RoMEO database to judge whether or not it is copyright safe to add this version of the paper to this repository.
http://www.swansea.ac.uk/iss/researchsupport/cronfa-support/

This is an open access article published under a Creative Commons Attribution (CC-BY) License, which permits unrestricted use, distribution and reproduction in any medium, provided the author and source are cited.

ACS APPLIED MATERIALS & INTERFACES

Research Article

www.acsami.org

Nondestructive Method for Mapping Metal Contact Diffusion in In_2O_3 Thin-Film Transistors

Olga Kryvchenkova,*[,†] Isam Abdullah,[‡] John Emyr Macdonald,[‡] Martin Elliott,[‡] Thomas D. Anthopoulos,[§] Yen-Hung Lin,[§] Petar Igić,[†] Karol Kalna,[†] and Richard J. Cobley[†]

[†]Electronic Systems Design Centre, Swansea University, Swansea SA1 8EN, U.K.

[‡]School of Physics and Astronomy, Cardiff University, The Parade, Cardiff CF24 3AA, U.K.

[§]Department of Physics and Centre for Plastic Electronics, Blackett Laboratory, Imperial College London, London SW7 2AZ, U.K.

Supporting Information

ABSTRACT: The channel width-to-length ratio is an important transistor parameter for integrated circuit design. Contact diffusion into the channel during fabrication or operation alters the channel width and this important parameter. A novel methodology combining atomic force microscopy and scanning Kelvin probe microscopy (SKPM) with self-consistent modeling is developed for the nondestructive detection of contact diffusion on active devices. Scans of the surface potential are modeled using physically based Technology Computer Aided Design (TCAD) simulations when the transistor terminals are grounded and under biased conditions. The simulations also incorporate the tip geometry to investigate its effect on the measurements due to electrostatic tip−sample interactions. The method is particularly useful for semiconductor− and metal−semiconductor interfaces where the potential contrast resulting from dopant diffusion is below that usually detectable with scanning probe microscopy.

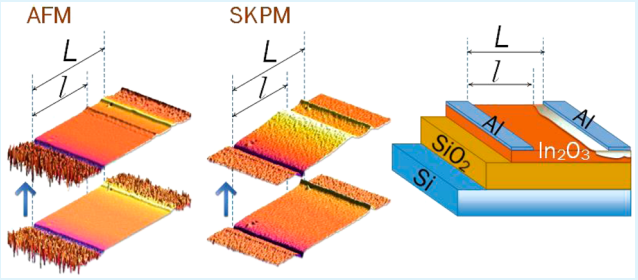

KEYWORDS: *AFM, Kelvin probe, In_2O_3, solution processing, metal oxide transistors*

1. INTRODUCTION

Atomic force microscopy (AFM) is a commonly used method for nondestructive mapping of sample topography[1] and is also an essential part of the commonly used double-pass scanning Kelvin probe microscopy (SKPM) method that allows measurement of the sample surface potential.[2−5] Using the known tip work function, a 2D map of the sample surface work function can then be reconstructed.[1−3] Measurements of the surface potential on operating transistors are complicated by mobile charges which are continuously created and transported across the device[6] and are influenced by the external field of the measuring probes. Therefore, the measurement result will include not only the intrinsic electrical properties of the sample but also measurement artifacts due to the presence of the tip.[6−10] This characterization technique is applied here to investigate In_2O_3 thin-film transistors (TFTs).[11−15]

SKPM is a well-established technique to study device interfaces.[16] Diffusion at the interface gives rise to nonabrupt potential distributions which can be used to assess the effect. Several authors have studied similar dopant diffusion problems with unbiased devices and structures, where potential offsets in the region of 100s of mV are detectable.[17,18] Here we focus on the detection of diffusion at a device interface which gives rise to low potential changes, which are difficult to detect with SKPM on unbiased samples.

In_2O_3 is a wide bandgap material with a cubic crystal structure.[19,20] The thin-film form has high transparency in the visible range (>90%), high electrical conductivity, and large-area uniformity. In_2O_3 is popular for potential device applications including liquid crystal displays, solar cells, and resistive memories.[11−14] In_2O_3 TFTs have also been proposed for high-resolution displays where it is preferable to have a large on-current to drive pixels and a low off-current for low power consumption. In_2O_3 TFTs on SiO_2/Si substrates and Al electrodes are typically bottom gate, normally on n-channel transistors[15] with a carrier mobility in the range from 0.4 to 23 $cm^2/V{\cdot}s$ and on−off ratio of $\sim 10^5-10^6$.[13,21−23] Al contacts are commonly used due to the electrical properties and cost, which give reliable, time-stable contacts.[24] One of the major drawbacks in using Al contacts is the formation of the native oxide and Al diffusion into the semiconductor material which can affect the contact reliability.[24−26]

In this paper we first present a method for using SKPM and AFM to determine diffusion regions in In_2O_3 TFTs, which give rise to potential shifts close to the detection threshold for standard AFM and SKPM. By applying a bias to the device, the unequal distribution of the applied potential between the

Received: August 17, 2016
Accepted: September 1, 2016
Published: September 1, 2016

 © 2016 American Chemical Society

DOI: 10.1021/acsami.6b10332
ACS Appl. Mater. Interfaces 2016, 8, 25631−25636

differently doped regions accentuates the difference, making the potential change easily detectable. We then explore the effects of gate bias and the interaction of the probe on this method. We investigate these effects and propose the most accurate method to nondestructively determine contact diffusion. We verify our results using 2D drift-diffusion simulations in Silvaco Atlas.[27] The diffusion alters the length of the channel, a crucial design parameter in transistor design, and is the cause of the higher output current observed in devices with a large contact diffusion area.

2. METHODS

2.1. Transistor Fabrication. A schematic of the bottom-gate In_2O_3 TFT operating under gate bias $V_{GS} > 0$ and drain bias $V_{DS} > 0$ is shown in Figure 1. The device has an aluminum source and drain

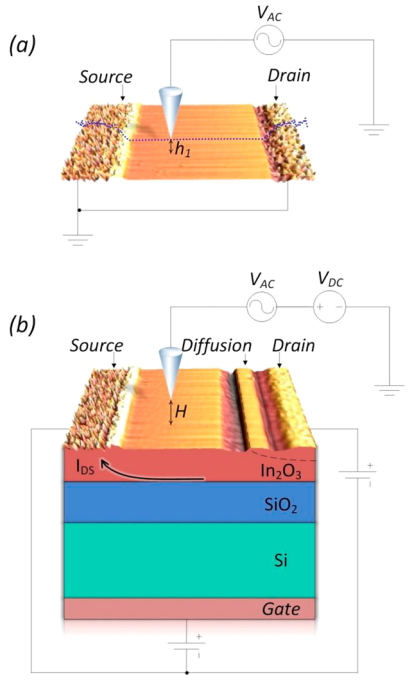

Figure 1. Combined measurement-schematic illustration of the SKPM double-pass method performed on a typical n-channel In_2O_3 TFT structure. (a) A 40 μm × 40 μm measured gradient map of the single-spin In_2O_3 TFT without bias and (b) the same at V_{DS} = 5 V and V_{GS} = 0 V revealing the position of the diffusion region as marked, with a schematic of the device structure below.

electrodes, a 100 nm thick SiO_2 dielectric layer, an In_2O_3 semiconducting channel layer, and a heavily doped n-type Si substrate layer, which serves as a gate electrode. The excessive indium atoms or oxygen vacancies serve as donors and make In_2O_3 an n-type semiconductor.[12,28] When positive drain voltages are applied, negative charge from the source electrode is injected, and an n-type conducting channel will be formed at the interface of the In_2O_3 layer with the SiO_2 gate dielectric, as shown in Figure 1(b).

Two In_2O_3 TFTs were selected for direct comparison. Figure 2 shows the $I-V$ characteristics of a single-spin TFT, for which a 4 nm In_2O_3 film results from a single spin-casting procedure.[22] The channel length $L \sim 30$ μm, and width $W \sim 1000$ μm. Figure 3 shows the corresponding $I-V$ characteristics for a film of thickness of 7−8 nm prepared by consecutive spin-casting of two layers of In_2O_3.[22] For this double-spin device, $L \sim 40$ μm and $W \sim 200$ μm. From the transfer characteristic of the double-spin device shown in Figure 3(b) one could estimate a threshold voltage value of 0.0 V, while the single-spin device threshold voltage could be estimated at 2.5 V[29,30] (see Figure 2(b)).

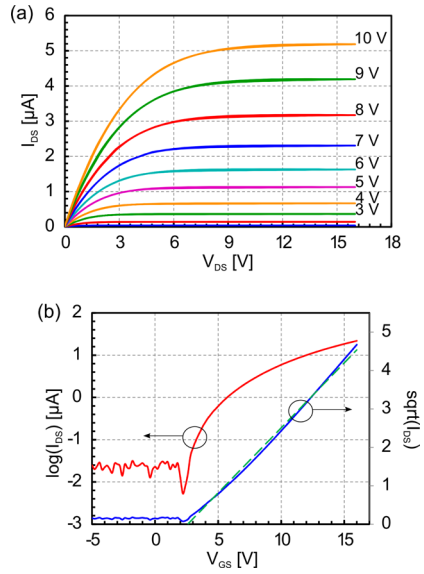

Figure 2. (a) Output characteristic at V_{GS} = 1 to 10 V with a step of 1 V. (b) Transfer characteristics in the saturation regime at V_{DS} = 10 V for the single-spin device.

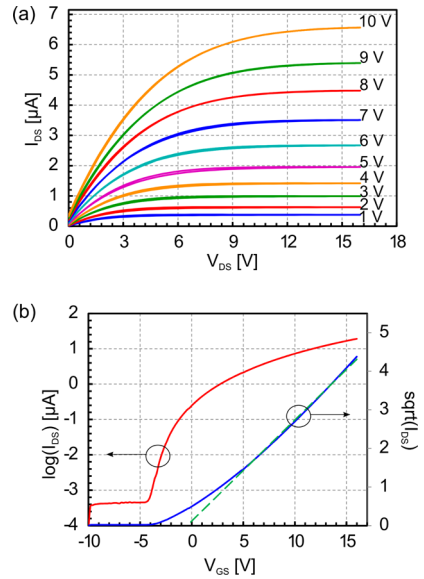

Figure 3. (a) Output characteristic at V_{GS} = 1 to 10 V with a step of 1 V. (b) Transfer characteristics in the saturation regime at V_{DS} = 10 V for the double spin device.

2.2. SKPM and AFM Measurement Methods. A double-pass SKPM method was performed on the In_2O_3 TFT in two stages, shown in Figure 1(a). During the first scan, surface topography is obtained in intermittent contact mode,[2,31] during which the cantilever vibration amplitude h_1 is maintained by a feedback loop.[1] An example of the reconstructed sample topography gradient for the single-spin device is shown in Figure 1(a) where source and drain electrodes can be clearly detected. To obtain the surface potential V_S in the second scan the tip is retracted at the constant lift height H = 20 nm (Figure 1(b)). It follows the line topography obtained in the first scan with the amplitude h_2, where $h_2 < h_1$. During the second scan a constant voltage $V_{DC} + V_{AC} \sin(\omega t)$ is applied to the tip with V_{DC} varied to minimize the amplitude of induced tip oscillations, so that the electrical potential in the channel can be measured (after correction for the contact potential difference between the tip and surface).[1,32,33] During the measurements the source electrode is always grounded. WSxM

DOI: 10.1021/acsami.6b10332
ACS Appl. Mater. Interfaces 2016, 8, 25631−25636

software is used to visualize the 2D measured AFM and SKPM profiles.[34]

2.3. Simulation Setup. The device structure shown in Figure 1(b) was modeled within Silvaco Atlas[27] which has been used by us to model coupled device-probe measurements under device operation.[35] In simulations, gate lengths of 25.62 μm (single spin) and 36.5 μm (double spin) are used with 70 μm Al source and drain electrodes, 4 nm (single spin) and 10 nm (double spin) n-type In_2O_3-conducting channel layer with a doping concentration of 8×10^{17} cm^{-3}, 100 nm SiO_2 insulator layer, and 300 nm n-type Si substrate layer with a doping concentration of 10^{20} cm^{-3} followed by a bottom Al gate. To simulate the contact diffusion regions around the drain and source electrodes, we use an n-type doping concentration of 2×10^{18} cm^{-3}. Other material parameters used in the simulations are In_2O_3 permittivity of 8.9,[36] bandgap of 4.0 eV,[11,12,20,28] electron affinity of 4.45 eV,[11] field-effect mobility of 0.27 cm^2/V × s, electron effective mass of $0.3m_0$[20], and tip work function of 4.6 eV. The Schottky barrier height of 0.7 eV is extracted from the measured profiles for the source and drain electrodes. The simulated devices have threshold voltages of −0.3 V for the double-spin transistor and 1.8 V for the single-spin transistor which is in good agreement with the measurements.

The structural quality of the interface between the In_2O_3 channel and dielectric material must be high to reduce scattering at the interface.[15] Charge-trapping effects in the channel layer have been reported to result in a decrease in the drain current when the drain bias is further increased.[15] In the present work, no current degradation is observed, and hence no charge-trapping effects are included in the simulation.

3. RESULTS AND DISCUSSION

3.1. Single-Spin Device. Figure 4(a) shows that the surface potential map at $V_{GS} = V_{DS} = 0$ V is flat and uniform through the channel with the averaged line scan shown beneath in Figure 4(b) where source and drain electrode edges can be seen at around 8 and 33 μm, respectively.

In Figure 4(b), the potential distribution through the In_2O_3 channel at $V_{DS} = 5$ V flattens in the region from 28 μm up until the previously determined edge of the drain electrode at 33 μm, in both the simulations and the experiment. Potential flattening suggests that this area is well-connected to the drain electrode by a low resistance path, consistent with a higher doping concentration after Al diffusion into the In_2O_3 channel. Simulations suggest that the doping concentration in the diffusion region increased from 2×10^{17} cm^{-3} to 8×10^{18} cm^{-3}. The edge of the diffusion region was estimated at 28.0 μm where the gradient of the surface lateral electric field (Figure 4(c)), calculated as a second derivative of the potential, has a local extremum. Analogously, using the data in Figure 4(b), the electrode edges at 7.7 and 33.3 μm were detected where the absolute change in the electric field has a local extremum. This gives a lateral diffusion width of 5.3 μm. Both profiles at $V_{DS} = 0$ V and $V_{DS} = 5$ V are in a very good agreement and give the same value of the electrode's edge position.

The position of the diffusion region edge can be determined only from the potential profiles of the biased device. It would not be possible to determine the diffusion region edge using the potential profile when TFT terminals are grounded ($V_{GS} = V_{DS} = 0$ V) in Figure 4(b) because the surface potential change will only depend on the intrinsic material parameters, In_2O_3 affinity of the channel layer, diffusion region, and Al work function. The potential drop between the In_2O_3 channel layer (with an estimated n-type doping concentration of 8×10^{17} cm^{-3}) and In_2O_3 diffusion region (with an estimated n-type doping concentration of 2×10^{18} cm^{-3}) is only 0.028 V as derived from the simulation results. This potential drop of 0.028 eV is below

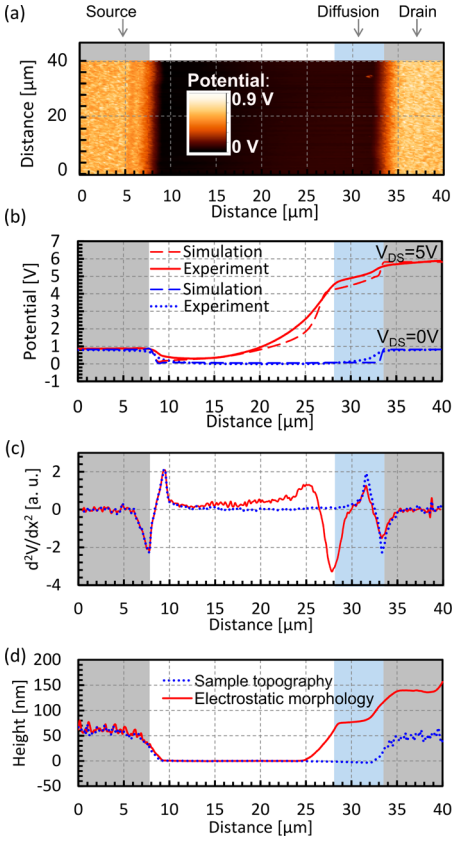

Figure 4. (a) Potential distribution at the surface when terminals of the single-spin TFT are grounded. Only the source and drain electrodes can be detected at 0 V. (b) Measured and simulated potential profiles at $V_{DS} = 0$ V and $V_{DS} = 5$ V when $V_{GS} = 0$ V. (c) Calculated second derivative of the measured surface potential at $V_{DS} = 0$ V (dashed line) and $V_{DS} = 5$ V (solid line) represents a measured change in the lateral electric field and allows determining exactly a diffusion region edge. (d) Measured electrostatic contribution to the apparent morphology and sample topography for a biased transistor corresponding to the potential profiles in (a).

the practical sensitivity of SKPM measurements on such samples.[37] Hence the diffusion edge cannot be detected in Figure 4(b) for the $V_{DS} = 0$ V profile due to the tip cone and cantilever averaging effect limiting measurement sensitivity.[7] The clear visibility of the diffused region arises from its high Al dopant concentration in the region close to the drain electrode, which would otherwise be depleted in the saturation regime of the TFT. This leads to a sharp gradient change in the potential profile at the boundary between the depleted channel and the Al-doped diffusion region.

The experiment and simulation show very good agreement, with the difference in potential around the edges of electrodes and diffusion within the error expected due to the cantilever contributions which average a contact potential in the vicinity of the tip apex during the experiment[7,33,38] (as the cantilever is not included in this simulation).

In light of the SKPM investigation, we found that AFM measurements along with a biased drain electrode can be used to identify the contact diffusion. When scanning above the uniformly charged diffusion region at $V_{DS} = 5$ V, the AFM tip will keep a constant height from 28 μm up until the edge of the drain electrode at about 33 μm. This apparent increase in height across the Al diffusion region and the electrode arises

DOI: 10.1021/acsami.6b10332
ACS Appl. Mater. Interfaces 2016, 8, 25631−25636

from the feedback loop compensating for the longer-range electrostatic interaction with the tip. The Al-diffusion region detected with this standard AFM topography scan with a biased drain electrode in Figure 4(d) corresponds well with the diffusion region detected with the SKPM results in Figure 4(b). The results obtained for a range of drain biases for V_{DS} > 2 V are shown in Figure S1 in the Supporting Information.

Due to the contact diffusion in single-spin TFTs the effective channel length L_{eff} was measured to be from 11% to 21% shorter than the measured source to drain distance L (see Table S1 in Supporting Information). The single-spin TFT with higher diffusion showed eight times higher output current due to the shorter L_{eff} and hence the effects of channel length reduction on the current.

3.2. Double-Spin Device. The measured and simulated surface potentials and tip height data for the double-spin device are presented in Figure 5. The measured SKPM profiles (V_{DS} = 8 V and V_{GS} = 0 V) in Figure 5(a) show potential flattening near the drain electrode due to diffusion which can be accurately allocated using the calculated lateral surface electric field in Figure 5(a). From Figure 5(a) the edge of the source and drain electrode can be detected at 4.7 and 41.2 μm, respectively, where Schottky barriers are formed between the Al contact and the In_2O_3 channel. The diffusion region in Figure 5(a) around the drain electrode can be identified at 37.7 μm because this is the edge of the high potential region which corresponds to the In_2O_3 semiconductor region with high dopant screening effect and can be related to the electrode diffusion. A peak in lateral electric field at 37.7 μm is created due to the potential drop between high potential diffusion region and In_2O_3 channel layer. Thereby a diffusion region of 3.5 μm can easily be detected using SKPM, narrower than the single-spin device diffusion width of 5.3 μm

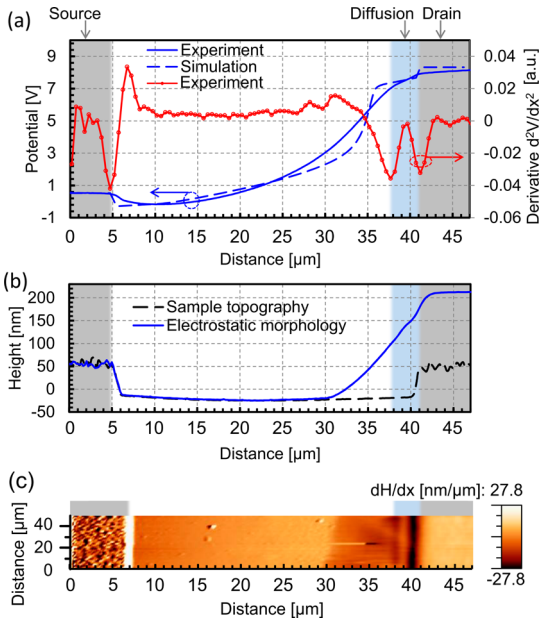

Figure 5. (a) Measured and simulated potential profile at V_{DS} = 8 V and V_{GS} = 0 V for the double-spin In_2O_3 TFT. The red line denotes the second differential of the potential. (b) A height line scan for V_{DS} = 0 V demonstrating the actual sample topography (black dash line), and a height line scan for V_{DS} = 8 V shows the same with the electrostatic contribution to the apparent morphology of the sample (blue solid line). (c) 2D distribution of the derivative of electrostatic contribution to the apparent morphology on the In_2O_3 TFT surface at V_{DS} = 8 V with the diffusion region marked.

During AFM scans of the double-spin In_2O_3 TFT presented in Figure 5(b), the electrostatic contribution to the apparent morphology was also measured when a drain bias of V_{DS} = 8 V and gate bias of V_{GS} = 0 V are applied. The sample topography obtained when the tip and transistor terminals are grounded is demonstrated in Figure 5(b) for a direct comparison and indicates that the channel layer is flat and free of voids and cracks. Both topography and electrostatic contribution to the apparent morphology profiles confirm the position of the source and drain electrodes and are in good agreement with the source and drain edges found from the SKPM profiles in Figure 5(a). The position of the diffusion region at 37.7 μm can be confirmed from the AFM data using profiles of the electrostatic contribution to the apparent morphology in Figure 5(b) and corresponding to the 2D map in Figure 5(c).

Due to the contact diffusion in the double-spin TFTs, the effective channel length L_{eff} was measured to be from 10% to 32% shorter than the measured source to drain distance L (see Table S1 in Supporting Information) and resulted in four times higher output current in the device with higher diffusion.

3.3. Effect of the Applied Gate Bias. The results presented so far to determine the extent of the contact diffusion do so without any applied gate bias. Here we explore the effect of using this method with a gate bias applied. In Figure 6 measured and simulated potential profiles are shown for the single-spin device at V_{DS} = 3 V and at the various gate biases: V_{GS} = 0 V and V_{GS} = 5 V. It has been suggested in the literature that a lower surface potential through the channel for organic field-effect transistors indicates a lower mobility in the device.[39] Applying a gate bias introduces more carriers into the channel, thus increasing the conductivity of the In_2O_3 channel.

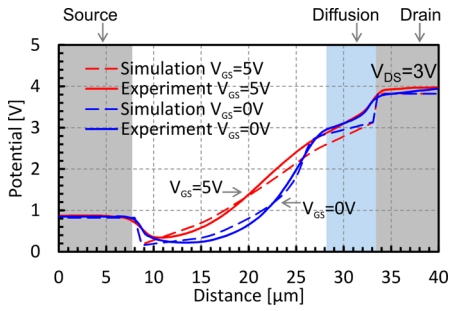

Figure 6. Measured and simulated potential profiles at V_{DS} = 3 V for the single-spin In_2O_3 TFT at V_{GS} = 0 V and V_{GS} = 5 V.

Figure 6 shows that simulated surface potential profiles are consistent with the measurement data for the single-spin device: the potential profile along the channel becomes more linear with increasing applied gate bias. For V_{GS} = 5 V, the channel is conducting throughout its length, and hence the effect of the additional Al doping in the diffused region close to the drain electrode is reduced, leading to a smaller change of the surface potential gradient at the edge of the diffusion region. Precise detection of the diffusion region edge with SKPM is easiest when the channel is depleted, i.e., when no gate bias is applied on the TFT.

3.4. Effect of the Electrostatic Interaction of the Scanning Probe with the Sample Surface. Here, we explore the effect of the scanning probe on the measurement of the diffusion region. Simulations of EFM and SKPM surface

DOI: 10.1021/acsami.6b10332
ACS Appl. Mater. Interfaces 2016, 8, 25631−25636

potential profiles with a full tip and cantilever structure have been demonstrated in the literature, where the tip-induced band bending was considered to be negligible.[6,40] When investigating semiconductor surfaces, the electrostatic force between the tip and sample is nullified by setting the contact potential difference (V_{CPD}) to be $V_{CPD} = V_{DC}$, and the tip-induced band bending at the sample surface is considered to be zero.[40] This approach to nullify the electrostatic force between the tip and the sample was shown to be valid for metal−metal infinite plates. However, this nulling is not always valid for a metal−semiconductor material system because the charge distribution within the semiconductor and within the n-type silicon tip will depend on the tip−sample separation.[4,41]

In this work a large change in the potential profiles for the higher drain biases (V_{DS} > 3 V) was observed due to the electrostatic interaction of the tip apex with the sample surface (Figure 7). The potential drops between the drain electrode,

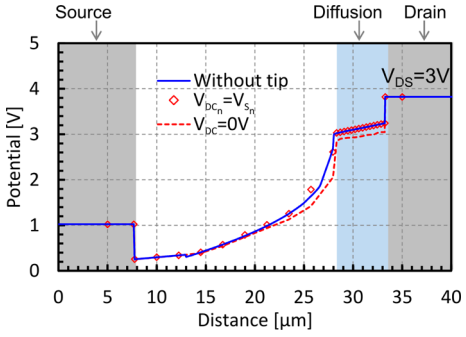

Figure 7. Simulation with 0 V bias on the tip (dashed line) and with the tip bias matched to the measured potential under the tip (open diamonds) at V_{DS} = 3 V. The potential profile with no tip present is also shown for comparison (blue line). The tip apex structure with an 80 nm radius and a 20 nm tip−sample separation are used.

diffusion region, and channel layer are additionally increased due to the presence of the scanning tip apex. However, when the tip bias is adjusted in the simulation to match the surface potential directly beneath the tip, as happens in experimental SKPM measurements, the effect of the tip interaction on the potential profile is minimal. More detail on the simulated probe−sample system is available in the Supporting Information.

4. CONCLUSION

Differential potential profile maps measured using SKPM and apparent morphology scans using AFM were used to measure contact diffusion into the channel of In_2O_3 TFTs. We show that using conventional AFM or SKPM on an unbiased sample will not reveal this structure adequately. We show that a drain bias must be applied for the diffusion region to be clearly detected as a sharp change in the potential profile gradient at the boundary between the depleted channel and the unintentionally doped region where contact diffusion occurs. Increasing the gate bias reduces the sensitivity of the method due to the accumulated charge along the length of the channel. Simulations of the electrostatic probe interaction indicate that the biased tip does not have a significant effect. We match all of our findings to simulations with very good agreement.

The methodology is applied to detect Al contact diffusion in In_2O_3 thin-film transistors, revealing a diffusion region as small as 3.5 μm, with the effective channel length decreasing by up to 32%. Al diffusion is also found to act as an additional n-type dopant, with an increase in the n-type doping concentration of the In_2O_3 layer from 2×10^{18} to 8×10^{18} cm^{-3}.

This approach can be applied generally to all semiconductor−semiconductor or semiconductor−metal interfaces, where interface diffusion is thought to be present but is below the detection threshold of standard AFM or SKPM.

■ ASSOCIATED CONTENT

Supporting Information

The Supporting Information is available free of charge on the ACS Publications website at DOI: 10.1021/acsami.6b10332.

Height line scans for V_{DS} from 0 to 3 V. The values of the drain current I_{DS}, channel length L, effective channel length L_{eff}, and diffusion region L_{diff} at V_{GS} = 10 V and V_{DS} = 16 V for the double-spin and single-spin In_2O_3 TFTs. Simulated tip movement and tip structure used in the simulation (PDF)

■ AUTHOR INFORMATION

Corresponding Author

*E-mail: o.kryvchenkova@swansea.ac.uk.

Notes

The authors declare no competing financial interest.

■ ACKNOWLEDGMENTS

IA thanks the Iraqi Cultural Attache for sponsorship and Salahaddin University for ongoing support. YHL and TDA are grateful to European Research Council (ERC) AMPRO project no. 280221 for financial support. OK would like to thank the Zienkiewicz Scholarship (Swansea University, UK) for financial support. The work was partially supported by EPSRC grant EP/K03099X/1.

■ REFERENCES

(1) Melitz, W.; Shen, J.; Kummel, A. C.; Lee, S. Kelvin Probe Force Microscopy and Its Application. *Surf. Sci. Rep.* **2011**, *66* (1), 1−27.
(2) Saive, R.; Scherer, M.; Mueller, C.; Daume, D.; Schinke, J.; Kroeger, M.; Kowalsky, W. Imaging the Electric Potential within Organic Solar Cells. *Adv. Funct. Mater.* **2013**, *23* (47), 5854−5860.
(3) Tello, M.; Chiesa, M.; Duffy, C. M.; Sirringhaus, H. Charge Trapping in Intergrain Regions of Pentacene Thin Film Transistors. *Adv. Funct. Mater.* **2008**, *18* (24), 3907−3913.
(4) Charrier, D. S. H.; Kemerink, M.; Smalbrugge, B. E.; de Vries, T.; Janssen, R. A. J. Real versus Measured Surface Potentials in Scanning Kelvin Probe Microscopy. *ACS Nano* **2008**, *2* (4), 622−626.
(5) Müller, K.; Goryachko, A.; Burkov, Y.; Schwiertz, C.; Ratzke, M.; Köble, J.; Reif, J.; Schmeißer, D. Scanning Kelvin Probe and Photoemission Electron Microscopy of Organic Source-Drain Structures. *Synth. Met.* **2004**, *146* (3), 377−382.
(6) Liscio, A.; Palermo, V.; Müllen, K.; Samorì, P. Tip−Sample Interactions in Kelvin Probe Force Microscopy: Quantitative Measurement of the Local Surface Potential. *J. Phys. Chem. C* **2008**, *112* (44), 17368−17377.
(7) Sacha, G. M.; Verdaguer, a.; Martínez, J.; Sáenz, J. J.; Ogletree, D. F.; Salmeron, M. Effective Tip Radius in Electrostatic Force Microscopy. *Appl. Phys. Lett.* **2005**, *86* (12), 123101.
(8) Valdrè, G.; Moro, D. 3D Finite Element Analysis of Electrostatic Deflection of Commercial and FIB-Modified Cantilevers for Electric and Kelvin Force Microscopy: I. Triangular Shaped Cantilevers with Symmetric Pyramidal Tips. *Nanotechnology* **2008**, *19* (40), 405501.
(9) Kryvchenkova, O.; Cobley, R. J.; Kalna, K. Self-Consistent Modelling of Tunnelling Spectroscopy on III−V Semiconductors. *Appl. Surf. Sci.* **2014**, *295*, 173−179.

DOI: 10.1021/acsami.6b10332
ACS Appl. Mater. Interfaces 2016, 8, 25631−25636

(10) Barnett, C. J.; Kryvchenkova, O.; Wilson, L. S. J.; Maffeis, T. G. G.; Kalna, K.; Cobley, R. J. The Role of Probe Oxide in Local Surface Conductivity Measurements. *J. Appl. Phys.* **2015**, *117* (17), 174306.
(11) Lang, O.; Pettenkofer, C.; Sánchez-Royo, J. F.; Segura, A.; Klein, A.; Jaegermann, W. Thin Film Growth and Band Lineup of In[sub 2]O[sub 3] on the Layered Semiconductor InSe. *J. Appl. Phys.* **1999**, *86* (10), 5687.
(12) King, P.; Veal, T.; Fuchs, F.; Wang, C.; Payne, D.; Bourlange, A.; Zhang, H.; Bell, G.; Cimalla, V.; Ambacher, O.; Egdell, R.; Bechstedt, F.; McConville, C. Band Gap, Electronic Structure, and Surface Electron Accumulation of Cubic and Rhombohedral In2O3. *Phys. Rev. B: Condens. Matter Mater. Phys.* **2009**, *79* (20), 205211.
(13) Park, J. H.; Yoo, Y. B.; Lee, K. H.; Jang, W. S.; Oh, J. Y.; Chae, S. S.; Lee, H. W.; Han, S. W.; Baik, H. K. Boron-Doped Peroxo-Zirconium Oxide Dielectric for High-Performance, Low-Temperature, Solution-Processed Indium Oxide Thin-Film Transistor. *ACS Appl. Mater. Interfaces* **2013**, *5* (16), 8067−8075.
(14) Street, R. A. Thin-Film Transistors. *Adv. Mater.* **2009**, *21* (20), 2007−2022.
(15) Jiao, Y.; Zhang, X.; Zhai, J.; Yu, X.; Ding, L.; Zhang, W. Bottom-Gate Amorphous In2O3 Thin Film Transistors Fabricated by Magnetron Sputtering. *Electron. Mater. Lett.* **2013**, *9* (3), 279−282.
(16) Henning, A. K.; Hochwitz, T.; Slinkman, J.; Never, J.; Hoffmann, S.; Kaszuba, P.; Daghlian, C. Two-Dimensional Surface Dopant Profiling in Silicon Using Scanning Kelvin Probe Microscopy. *J. Appl. Phys.* **1995**, *77* (5), 1888.
(17) Shin, H.; Kim, C.; Lee, B.; Kim, J.; Park, H.; Min, D.-K.; Jung, J.; Hong, S.; Kim, S. Formation and Process Optimization of Scanning Resistive Probe. *J. Vac. Sci. Technol. B Microelectron. Nanom. Struct.* **2006**, *24* (5), 2417.
(18) Koren, E.; Berkovitch, N.; Rosenwaks, Y. Measurement of Active Dopant Distribution and Diffusion in Individual Silicon Nanowires. *Nano Lett.* **2010**, *10* (4), 1163−1167.
(19) Sato, Y.; Otake, F.; Hatori, H. A Dependence of Crystallinity of In2O3 Thin Films by a Two-Step Heat Treatment of Indium Films on the Heating Atmosphere. *J. Mod. Phys.* **2010**, *01* (06), 360−363.
(20) Robertson, J.; Falabretti, B. *Handbook of Transparent Conductors*; Ginley, D. S., Ed.; Springer US: Boston, MA, 2011.
(21) Liu, A.; Liu, G. X.; Zhu, H. H.; Xu, F.; Fortunato, E.; Martins, R.; Shan, F. K. Fully Solution-Processed Low-Voltage Aqueous In2O3 Thin-Film Transistors Using an Ultrathin ZrOx Dielectric. *ACS Appl. Mater. Interfaces* **2014**, *6* (20), 17364−17369.
(22) Lin, Y.-H.; Faber, H.; Labram, J. G.; Stratakis, E.; Sygellou, L.; Kymakis, E.; Hastas, N. A.; Li, R.; Zhao, K.; Amassian, A.; Treat, N. D.; McLachlan, M.; Anthopoulos, T. D. High Electron Mobility Thin-Film Transistors Based on Solution-Processed Semiconducting Metal Oxide Heterojunctions and Quasi-Superlattices. *Adv. Sci.* **2015**, *2* (7), 1500058.
(23) Faber, H.; Lin, Y.-H.; Thomas, S. R.; Zhao, K.; Pliatsikas, N.; McLachlan, M. A.; Amassian, A.; Patsalas, P. A.; Anthopoulos, T. D. Indium Oxide Thin-Film Transistors Processed at Low Temperature via Ultrasonic Spray Pyrolysis. *ACS Appl. Mater. Interfaces* **2015**, *7* (1), 782−790.
(24) Kumm, J.; Chacko, R. V.; Samadi, H.; Hartmann, P.; Eberlein, D.; Jäger, U.; Wolf, A. Long-Term and Annealing Stable, Solderable PVD Metallization with Optimized Al Diffusion Barrier. *Energy Procedia* **2015**, *77*, 374.
(25) Kolawa, E.; Garland, C.; Tran, L.; Nieh, C. W.; Molarius, J. M.; Flick, W.; Nicolet, M.-A.; Wei, J. Indium Oxide Diffusion Barriers for Al/Si Metallizations. *Appl. Phys. Lett.* **1988**, *53* (26), 2644.
(26) Armigliato, A.; Valdré, G. Analytical Electron Microscopy of Al/TiN Contacts on Silicon for Applications to Very Large Scale Integrated Devices. *J. Appl. Phys.* **1987**, *61* (1), 390.
(27) *Atlas User's Manual*; 2007.
(28) Girtan, M.; Rusu, G. On the Size Effect in In_2O_3 Thin Films. *Mater. Sci. Eng., B* **1999**, 166−172.
(29) Zhuang, J.; Lo, W.-S.; Zhou, L.; Sun, Q.-J.; Chan, C.-F.; Zhou, Y.; Han, S.-T.; Yan, Y.; Wong, W.-T.; Wong, K.-L.; Roy, V. a. L. Photo-Reactive Charge Trapping Memory Based on Lanthanide Complex. *Sci. Rep.* **2015**, *5*, 14998.
(30) Huang, T.-S.; Su, Y.-K.; Wang, P.-C. Study of Organic Thin Film Transistor with Polymethylmethacrylate as a Dielectric Layer. *Appl. Phys. Lett.* **2007**, *91* (9), 092116.
(31) Schönherr, H.; Vancso, G. J. *Scanning Force Microscopy of Polymers*; Springer Berlin Heidelberg: Berlin, Heidelberg, 2010.
(32) Riedel, C.; Schwartz, G. a; Arinero, R.; Tordjeman, P.; Lévêque, G.; Alegría, a; Colmenero, J. Nanoscale Dielectric Properties of Insulating Thin Films: From Single Point Measurements to Quantitative Images. *Ultramicroscopy* **2010**, *110* (6), 634−638.
(33) Bayerl, D. J.; Wang, X. Three-Dimensional Kelvin Probe Microscopy for Characterizing In-Plane Piezoelectric Potential of Laterally Deflected ZnO Micro-/Nanowires. *Adv. Funct. Mater.* **2012**, *22* (3), 652−660.
(34) Horcas, I.; Fernández, R.; Gómez-Rodríguez, J. M.; Colchero, J.; Gómez-Herrero, J.; Baro, A. M. WSXM: A Software for Scanning Probe Microscopy and a Tool for Nanotechnology. *Rev. Sci. Instrum.* **2007**, *78* (1), 013705.
(35) Lord, A. M.; Maffeis, T. G.; Kryvchenkova, O.; Cobley, R. J.; Kalna, K.; Kepaptsoglou, D. M.; Ramasse, Q. M.; Walton, A. S.; Ward, M. B.; Köble, J.; Wilks, S. P. Controlling the Electrical Transport Properties of Nanocontacts to Nanowires. *Nano Lett.* **2015**, *15* (7), 4248−4254.
(36) Hamberg, I.; Granqvist, C. G. Evaporated Sn-Doped In2O3 Films: Basic Optical Properties and Applications to Energy-Efficient Windows. *J. Appl. Phys.* **1986**, *60* (11), R123.
(37) Li, C.; Minne, S.; Hu, Y.; Ji, M.; He, J.; Mittel, H.; Kelly, V.; Erina, N.; Guo, S.; Mueller, T. Peak Force Kelvin Probe Force Microscopy. *Bruker Appl. Note #* **2013**, *140*, 1−14.
(38) Sacha, G. M.; Sáenz, J. J. Cantilever Effects on Electrostatic Force Gradient Microscopy. *Appl. Phys. Lett.* **2004**, *85* (13), 2610.
(39) Lüttich, F.; Lehmann, D.; Friedrich, M.; Chen, Z.; Facchetti, A.; von Borczyskowski, C.; Zahn, D. R. T.; Graaf, H. Interface Properties of OFETs Based on an Air-Stable N-Channel Perylene Tetracarboxylic Diimide Semiconductor. *Phys. Status Solidi A* **2012**, *209* (3), 585−593.
(40) Zerweck, U.; Loppacher, C.; Otto, T.; Grafström, S.; Eng, L. Accuracy and Resolution Limits of Kelvin Probe Force Microscopy. *Phys. Rev. B: Condens. Matter Mater. Phys.* **2005**, *71* (12), 125424.
(41) Hudlet, S.; Saint Jean, M.; Roulet, B.; Berger, J.; Guthmann, C. Electrostatic Forces between Metallic Tip and Semiconductor Surfaces. *J. Appl. Phys.* **1995**, *77* (7), 3308.

DOI: 10.1021/acsami.6b10332
ACS Appl. Mater. Interfaces 2016, 8, 25631−25636